Topological constraints on the dynamics of vortex formation in a bi-dimensional quantum fluid

T. Congy,[1] P. Azam,[2] R. Kaiser,[2] and N. Pavloff[3,4]

[1] *Department of Mathematics, Physics and Electrical Engineering, Northumbria University, Newcastle upon Tyne NE1 8ST, United Kingdom*
[2] *Institut de Physique de Nice, Université Côte d'Azur, CNRS, F-06560 Valbonne, France*
[3] *Université Paris-Saclay, CNRS, LPTMS, 91405, Orsay, France*
[4] *Institut Universitaire de France (IUF)*

We present experimental and theoretical results on formation of quantum vortices in a laser beam propagating in a nonlinear medium. Topological constrains richer that the mere conservation of vorticity impose an elaborate dynamical behavior to the formation and annihilation of vortex/anti-vortex pairs. We identify two such mechanisms, both described by the same fold-Hopf bifurcation. One of them is particularly efficient although it is not observed in the context of liquid helium films or stationary linear systems because it relies on the finite compressibility and on the non-stationnarity of the fluid of light we consider.

It has been long understood that the propagation of light in a nonlinear medium can be described as a (dispersive) hydrodynamic phenomenon. This approach, pioneered in the 60's [1–6] and further developed in the 90's [7–10] yielded remarkable successes: observation of bright [11–13], dark [14–17] cavity [18, 19] and oblique [20, 21] solitons, of wave breaking and dispersive shock waves [22–26], of quantized vortices [27–36] and superfluid flow of light [37, 38]. An extreme hydrodynamic-like behavior is the turbulent regime in which typical observables display scale-invariant power law spectra in momentum space. In the present study we focus on two dimensional configurations, similar to those already studied in the field of Bose-Einstein condensates, where quantum vortices proliferation but also robust vortex structures have been observed [39–42]. Although their role in the different types of power laws which have been predicted and/or observed [39, 43, 44] is not fully elucidated [45–47], it makes no doubt that understanding the dynamics of vortex formation is crucial for unraveling the mechanisms leading to quantum turbulence. Recent studies have demonstrated the efficiency of optical platforms for studying this subject [48–54].

In the present work we use a nonlinear optical platform [26, 55, 56] for studying the formation and annihilation of vortices and of other less conspicuous features, such as saddles and phase extrema which also carry a topological charge. Although the existence of these other critical points has a long history [57, 58] their role in enforcing topological constrains [59–62] is often overlooked. The detection tool at our disposal is able to simultaneously record the intensity and the phase of the light issued from a nonlinear medium, making it possible to reconstruct the streamlines of the flow of the fluid of light, as illustrated in Fig. 1. This enables to investigate the formation mechanisms of vortices and critical points. In particular we experimentally demonstrate for the first time a scenario of vortex/anti-vortex formation first proposed by Nye *et al.* in 1988 [63] and identify a new one, which appears simpler and presumably more efficient in the context of turbulence of a compressible quantum fluid.

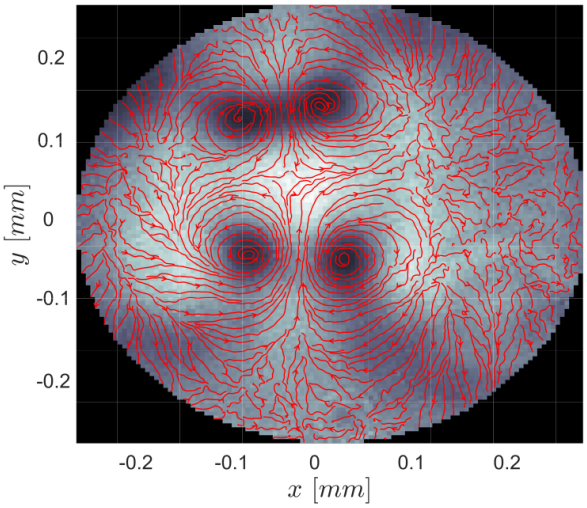


FIG. 1. Experimental intensity pattern and streamlines (in red) of the beam at the exit of the nonlinear vapor. Dark regions are of lesser intensity. One distinctly discerns two vortex/anti-vortex pairs and also a saddle located close to the origin.

Consider a quantum fluid described by a scalar order parameter of the form

$$\psi(\vec{r}) = A(\vec{r}) \exp[iS(\vec{r})], \tag{1}$$

defined in the plane ($\vec{r} = x\,\vec{e}_x + y\,\vec{e}_y$). In such a system the formation of vortices is constrained by topological rules: it is for instance well known that in the absence of externally imparted angular momentum, vortices typically appear in pairs with opposite quantized vorticity. This scenario is enriched by other constrains [63] originating from the fact that, to any closed curve C of the plane, are associated not one, but *two* topological indices: the

vorticity $I_{\rm V}(C) = \frac{1}{2\pi}\oint_C \mathrm{d}S$ and also the Poincaré-Hopf index $I_{\rm P}(C) = \frac{1}{2\pi}\oint_C \mathrm{d}\theta$, where θ is a polar angle of the "velocity field" $\vec{v}(\vec{r}) = \vec{\nabla}S$ and in both cases the integral is performed clockwise. $I_{\rm V}$ and $I_{\rm P}$ are (positive or negative) integers. This stems from the fact that along a close contour the phase S of the order parameter (1) and the orientation θ of the velocity must both vary by integer multiples of 2π [64]. If S is regular and well-defined in the interior of C, then $I_{\rm V}(C) = 0$. This value does not change unless a vortex [65] crosses C. To each vortex one can associate a vorticity and a Poincaré-Hopf index by integrating over a small circle around the vortex core. This leads to $I_{\rm P} = +1$ and typically [66] $I_{\rm V} = \pm 1$ for each vortex. Besides vortices, other points are also associated with a finite Poincaré-Hopf index: those at which the velocity of the flow cancels. They are known as critical points or equilibria. For a potential flow such as ours, where the phase S is the velocity potential, they are of two types: phase extrema (local maxima or local minima) and phase saddles. For an extremum $I_{\rm P} = +1$ and for a saddle $I_{\rm P} = -1$ [67], while for both $I_{\rm V} = 0$ [68]. Similarly to what occurs for the vorticity, the value $I_{\rm P}(C)$ does not change unless a critical point with non zero Poincaré-Hopf index (a vortex, a saddle or an extremum) crosses C.

The above topological considerations are generic and apply to any system described by a complex scalar order parameter. The physical implementation we consider in this Letter consists in the the propagation of a linearly polarized laser beam of wavelength $\lambda_0 = 2\pi/k_0 = 780$ nm in a cell filled with a nonlinear medium consisting in a natural Rb vapor at a temperature $T \approx 120°$. Within the paraxial approximation, denoting as z the coordinate along the beam axis and $\vec{r}$ the transverse coordinate, this propagation is described by a complex scalar field $\psi(\vec{r}, z)$ which obeys a generalized nonlinear Schrödinger equation [69] where z plays the role of an effective time:

$$i\,\partial_z\psi = -\frac{1}{2n_0k_0}(\partial_x^2+\partial_y^2)\psi + k_0n_2|\psi|^2\,\psi - \frac{i}{2\,\Lambda_{\rm abs}}\,\psi, \quad (2)$$

$|\psi|^2$ being the intensity, expressed in W.mm^{-2}. $\Lambda_{\rm abs}$ describes the effects of absorption: if $\mathcal{T}$ denotes the coefficient of energy transmission, then $\Lambda_{\rm abs} = -z_{\rm max}/\ln(\mathcal{T})$, where $z_{\rm max} = 7$ cm is the total length of propagation through the vapor. n_0 is the refractive index of the medium and n_2 is the nonlinear Kerr coefficient. The values of the parameters are $\mathcal{T} = 0.16$, $n_0 = 1$ and $n_2 = 2.2\times10^{-4}$ W^{-1}.mm^2 [70].

For studying the above discussed topological constrains we use a specifically designed incident light pattern which consists in the superposition of a main Gaussian beam (wide and isotropic) with an auxiliary one, more tightly focused and anisotropic. The initial amplitude can accordingly be written as

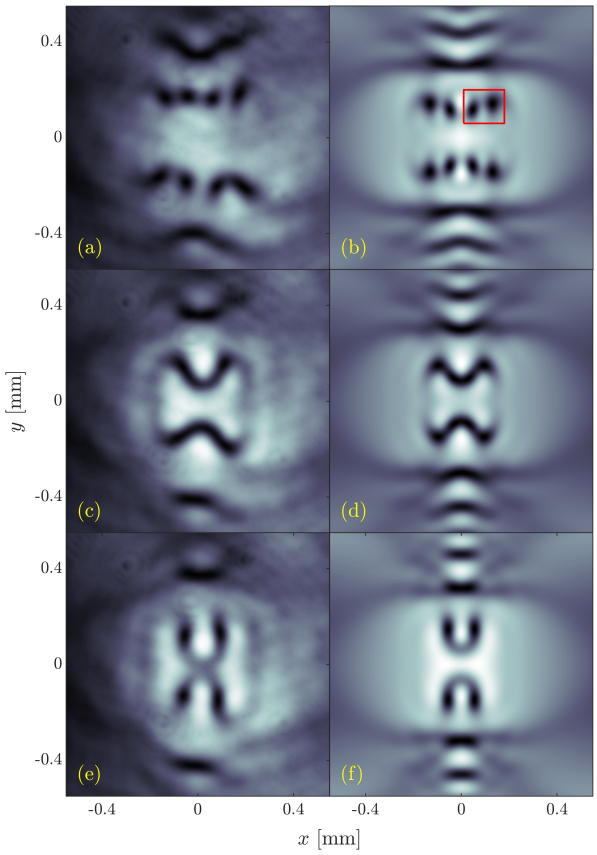


FIG. 2. Comparison of experimental measurements (left plots) and simulations (right plots) of the beam intensity pattern at the exit of the vapor ($z = 7$cm). The initial amplitude is given by (2) with $\Phi_2 = 0.96\,\pi$ in panels (a) and (b); $\Phi_2 = \pi$ in panels (c) and (d) and $\Phi_2 = 1.05\,\pi$ in panels (e) and (f). The red rectangle in panel (b) marks the location of a vortex/anti-vortex pair which formation is analysed below, see Fig. 3.

$$\psi(\vec{r},0) = \sqrt{I_1}\exp\left(-\frac{r^2}{w_{\rm G}^2}\right) + \sqrt{I_2}\exp\left(-\frac{x^2}{w_x^2}-\frac{y^2}{w_y^2}\right)\exp\{i\,\varphi_2(\vec{r})\}, \quad (3)$$

where $r = |\vec{r}|$, $w_{\rm G} = 1.1$ mm, $w_x = 0.55$ mm, $w_y = 0.08$ mm and $I_1 = I_2 = 0.4$ W.mm^{-2}. The initial phase of the auxiliary beam reads $\varphi_2(\vec{r}) = -k_0r^2/R_2 + \Phi_2$, where $R_2 = -0.5$ m is the initial curvature of the wavefront of the auxiliary beam and Φ_2 is the global phase difference between the auxiliary and the main beam. An antiphase relationship ($\Phi_2 = \pi$) corresponds to an intensity dip induced by the narrow auxiliary beam on the wide main one. We image the beam pattern at the exit of the cell for different initial phase differences Φ_2. This is performed thanks to a wave-front sensor which captures the amplitude and phase of the near field at the output of the nonlinear medium. As exemplified in Fig. 1 this offers the possibility to simultaneously measure the intensity and phase of the field, corresponding to the output opti-

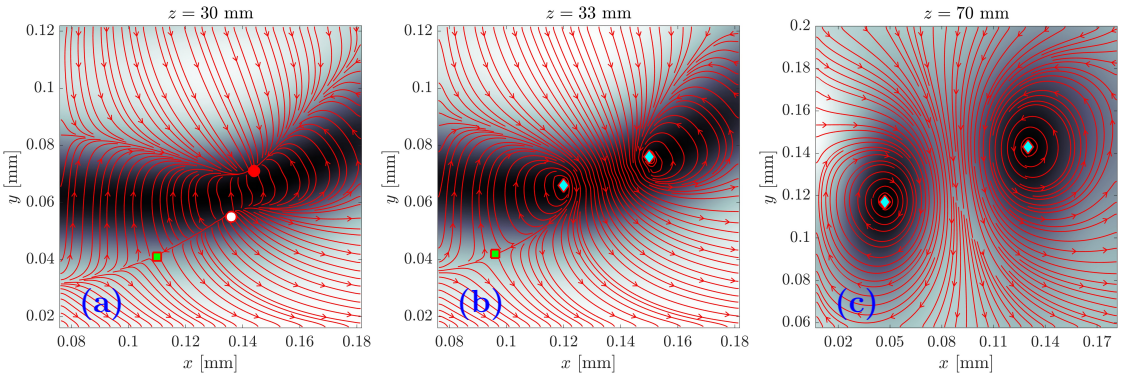


FIG. 3. Snapshots of simulations of the intensity pattern at several propagation distances within the nonlinear vapor. The initial profile is (3) with $\Phi_2 = 0.96\,\pi$. The corresponding final intensity pattern is represented in Fig. 2(b) of which plot (c) is a blow up. Regions of low intensity are dark. The oriented curves are the streamlines spanned by the vector field $\vec{v}(\vec{r})$. A red (white) circle locates a phase maximum (minimum), i.e., a stable (unstable) node. Cyan diamonds are vortices. The green square is a saddle which plays no part in the vortex formation mechanism.

cal fluid intensity $|\psi|^2$ and velocity $\vec{v}$ in our experiment.

Fig. 2 compares the experimental and theoretical intensity profiles $|\psi(x, y, z_{\max})|^2$ at the exit of the cell. In panels (a) and (b) eight vortices distributed symmetrically with respect to the horizontal and vertical axes are observed which have been created during the nonlinear propagation within the cell. When increasing the initial phase difference Φ_2 between the main and auxiliary beam, the vortices close to the y axis get even closer [panels (c) and (d)] and eventually merge [panels (e) and (f)]. The agreement between the experimental and numerical results displayed in Fig. 2 is excellent, especially if one considers that there are no free parameters: all the constants of the model have been determined by independent experimental measurements [70]. This validates the use of the nonlinear Schrödinger equation (2) for studying the intermediate steps ($0 < z < z_{\max}$) which are not accessible in our experiment.

The dynamics of the critical points during the propagation within the nonlinear vapor can be very complex, but it always fulfills the previously stated topological requirements. For instance, in numerical simulations, we have observed the concomitant apparition of a phase saddle and of a phase extremum, a process which preserves the total Poincaré-Hopf index. In a similar way, the topological rules impose that the annihilation of a vortex/anti-vortex pair be associated to the simultaneous disappearance of two saddles in order to ensure the conservation not only of I_{V} but also of I_{P}. This is the process at play in the disappearance of the two pairs of central vortices observed in Fig. 2, when going from the top to the bottom row. We will not go in the particulars of this mechanism here (see however the discussion in [70]) because it has been described in detail by the Bristol team [63] and also because it is seldom observed in our investigation. In the following we describe an alternative mechanism of vortex formation, much more often encountered in our setting: two phase extrema collide and annihilate one the other, giving birth to a vortex/anti-vortex pair. During this process the total Poincaré-Hopf index and total vorticity keep the value 2 and 0, respectively. This mechanism is at the origin of the formation of the two vortices in the red square of Fig. 2(b). Numerically computed intermediate beam structures leading to the output pattern shown in Figs. 2(a) and 2(b) are presented in Fig. 3. A phase minimum (white dot) approaches a phase maximum (red dot), pinching a low density region. The two extrema annihilate each other giving birth to a vortex/anti-vortex pair [cyan diamonds in Fig. 3(b)]. The fact that the two vortices have opposite vorticity is clearly seen from the orientation of the streamlines in the vicinity of each of them. After their formation, the two vortices slowly drift apart, eventually reaching in Fig. 3(c) the configuration identified by a red rectangle in Fig. 2(b).

The structure of the flow, entailed in the velocity field $\vec{v}(\vec{r})$, can be interpreted within the theory of dynamical systems by considering streamlines (red lines in Figs. 1 and 3) as trajectories of a two dimensional system:

$$\frac{\mathrm{d}\vec{r}}{\mathrm{d}\gamma} = \vec{v}(\vec{r}), \tag{4}$$

with γ an arbitrary parametrization on the trajectory. In the terminology of dynamical systems, phase extrema are known as nodes (stable or unstable) and saddles as saddle points [71]. Although vortices are not equilibria of the velocity field, the streamlines encircling a vortex are closed trajectories, and vortices can be seen as "centers" of the dynamical system (4). Within this framework, the change of topology of the flow can be viewed as a bifurcation of (4): for instance, the above mentioned concomitant apparition of a saddle point (phase saddle) and of a node (phase extremum) is described by a so-called saddle-node bifurcation. In the same line, the mechanism described previously, and displayed in Fig. 3, appears in the fold-Hopf bifurcation [72, 73] for which a generic normal form is given explicitly in [70]. For the

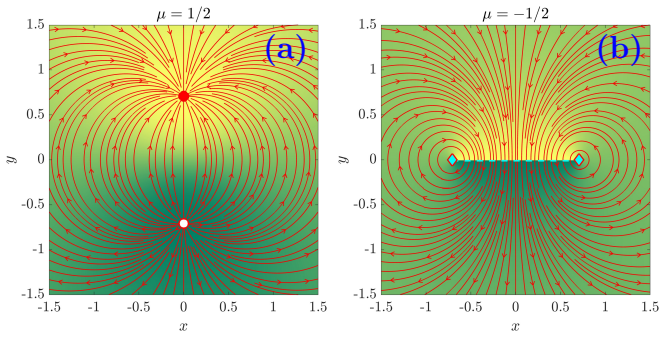


FIG. 4. Phase portraits of the dynamical system (4),(5) [or equivalently with (4),(6)] with $\sigma = 1$ for two different values of the bifurcation parameter μ. The color scale corresponds here to the phase $S_{\rm fH} \in [-\pi, \pi]$ (light yellow corresponds to $S_{\rm fH} = \pi$ and dark green to $S_{\rm fH} = -\pi$). Note that the position of the 2π-jump of $S_{\rm fH}(\vec{r})$ [dashed line in panel (b)], is arbitrary and fixed by the choice of constant of integration in (6).

present discussion it suffices to consider the system (4) with the specific form:

$$\vec{v} = \vec{v}_{\rm fH}(\vec{r}) \equiv -2\sigma xy\,\vec{e}_x + (\mu + \sigma x^2 - y^2)\,\vec{e}_y, \quad (5)$$

where $\sigma = \pm 1$ is fixed, and $\mu \in \mathbb{R}$ is a parameter of the bifurcation. The phase portrait of the dynamical system (4),(5) for $\sigma = 1$ and two different values of μ (before and after the bifurcation) is shown in Fig. 4. In this case, the stable and unstable nodes (red and white dot respectively) which exist when $\mu > 0$ annihilate when μ becomes negative to form two centers (represented by cyan diamonds); note that the latter are not singularities but true equilibria of the velocity field (5). The transition observed in the phase portraits of Fig. 4 by varying μ qualitatively compares to the flow patterns obtained in Figs. 3(a) and 3(b) by varying z.

The velocity field (5) is not that of a potential flow, as should be the case for a quantum fluid. However, it is possible to derive a potential flow which shares the same phase portrait. The corresponding velocity field reads (see [70])

$$\vec{v} = \vec{\nabla} S_{\rm fH}, \quad S_{\rm fH}(\vec{r}) \equiv \arg\left[x^2 + \sigma(y^2 + \mu) + i\sigma y\right]. \quad (6)$$

The system (4),(6) is not only a gradient flow, it also obeys the Onsager-Feynman quantization condition [64]. In particular the centers of (4),(5) are replaced by singularities (where $S_{\rm fH}$ is ill-defined) that are encircled by closed orbits along which the circulation of $\vec{\nabla} S_{\rm fH}$ is $\pm 2\pi$ [as depicted in Fig. 4(b)], i.e., quantum vortices. It is important to note that $S_{\rm fH}$ is not the phase of a wave-function which exactly obeys the nonlinear Schrödinger equation (2). However, varying μ in (6) effectively reproduce the local flow pattern of a z-varying wave-function solving (2). Besides, $S_{\rm fH}$ fulfills all the requirements expected from the phase of the order parameter (1) of a two-dimensional quantum fluid.

It is interesting to remark that the normal form (5), once modified to derive from the velocity potential (6) as just explained, also describes when $\sigma = -1$ the scenario of vortex annihilation presented in [63] which we henceforth denote as the Bristol mechanism: two vortices and two saddle points annihilate when μ goes from positive to negative, yielding a featureless flow. Notably, the model wavefunction given in [63] reduces to $\psi = x^2 - y^2 - \mu - iy$ close to the bifurcation point (see [70]), i.e., its phase is $S_{\rm fH}$ with $\sigma = -1$, validating the analogy presented here: the normal form of the fold-Hopf bifurcation provides an approximated theoretical model of the Bristol mechanism.

The mechanism of vortex formation illustrated in Figs. 3 and 4, although generic, cannot be observed in the special case of an incompressible bi-dimensional quantum fluid, such as commonly used to model liquid helium films for instance. Indeed, in such a system the phase S is a harmonic function, which, by the maximum principle cannot have maxima nor minima: the only possible critical points with zero velocity are saddles and no phase extrema occur, contrarily to what is observed in Fig. 3 (see an extended discussion of this point in [70]). Phase extrema are also forbidden in a stationary (i.e., z-independent in our case) system, as proven in Ref. [63], but nothing prevents their formation in a z-dependent configuration. Indeed, such extrema have been theoretically considered [59] and experimentally observed in a random linear speckle pattern [74], but were found to be relatively scarce, being outnumbered in a ratio 14:1 by saddles. Although our use of a specific initial condition (3) prevents a systematic statistical study (cf. [59] for a detailed discussion), we also observe that phase extrema are less numerous than saddles. This corresponds to physical intuition: extrema are typically born in saddle-node bifurcations which create an equal number of extrema and saddles, whereas pairs of saddles could be additionally created thanks to the Bristol mechanism. More significantly, the new mechanism of vortex formation we have identified and observed in many instances, efficiently diminishes the number of extrema. As a result, when vortices proliferate, saddles tend to be more numerous than extrema.

In conclusion we emphasize that our experimental apparatus pertains to a new generation of optical techniques which enable a precise measure of both the intensity and the phase of a light sheet [32, 35, 36, 52–54]. As demonstrated in the present Letter, this offers the possibility of an accurate and simple location not only of vortices but also of other critical points, such as saddles. This enabled us to obtain evidences of several (topologically constrained) mechanisms of vortex formation and of associated singular points in the time domain, with an account of the evolution of the streamlines. As far as vortex formation is concerned, we experimentally demonstrated a scenario proposed more than 30 year ago (the Bristol

mechanism). We also identified a new scenario, simpler and more common in our setting, in which two nodes collide and give birth to a vortex/antivortex pair. This process requires a non stationary flow and a system with finite (or zero) compressibility. We showed that the two mechanisms of vortex formation (Bristol and nodes collision) pertain to the same fold-Hopf type of bifurcation. We demonstrated that the corresponding normal form can be enriched in order to account for the quantum nature of our system. As a final remark we stress that our study illustrates the efficiency of tools issued from the theory of dynamical systems to investigate the route to turbulence. This opens the path of a new line of research devoted to the statistical study of nodes and saddles dynamics in a turbulent quantum fluid.

TC and NP would like to thank the Isaac Newton Institute (INI) for Mathematical Sciences for support and hospitality during the programme "Dispersive hydrodynamics: mathematics, simulation and experiments, with applications in nonlinear waves" when part of the work on this paper was undertaken. The work of TC was partially supported by the Simons Fellowships during the INI Programme.

[1] R. Y. Chiao, E. Garmire, and C. H. Townes, Self-trapping of optical beams, Phys. Rev. Lett. **13**, 479 (1964).
[2] V. I. Talanov, Self focusing of wave beams in nonlinear media, JETP Lett. **2**, 138 (1965).
[3] P. L. Kelley, Self-focusing of optical beams, Phys. Rev. Lett. **15**, 1005 (1965).
[4] V. I. Talanov, Self-modeling wave beams in a nonlinear dielectric, Sov. Radiophys. **9**, 260 (1966).
[5] S. A. Akhmanov, A. P. Sukhorukov, and R. V. Khokhlov, Self-focusing and self-trapping of intense light beams in a nonlinear medium, Sov. Phys. JETP **23**, 1025 (1966).
[6] S. A. Akhmanov, A. P. Sukhorukov, and R. V. Khokhlov, Self-focusing and diffraction of light in a nonlinear medium, Sov. Phys. Usp. **10**, 609 (1968).
[7] P. Coullet, L. Gil, and F. Rocca, Optical vortices, Opt. Commun. **73**, 403 (1989).
[8] M. Brambilla, L. A. Lugiato, V. Penna, F. Prati, C. Tamm, and C. O. Weiss, Transverse laser patterns. ii. variational principle for pattern selection, spatial multistability, and laser hydrodynamics, Phys. Rev. A **43**, 5114 (1991).
[9] Y. Pomeau and S. Rica, Diffraction non-linéaire, C. R. Acad. Sci. Paris série II, **317**, 1287 (1993).
[10] K. Staliunas, Laser Ginzburg-Landau equation and laser hydrodynamics, Phys. Rev. A **48**, 1573 (1993).
[11] J. E. Bjorkholm and A. A. Ashkin, cw self-focusing and self-trapping of light in sodium vapor, Phys. Rev. Lett. **32**, 129 (1974).
[12] L. F. Mollenauer, R. H. Stolen, and J. P. Gordon, Experimental observation of picosecond pulse narrowing and solitons in optical fibers, Phys. Rev. Lett. **45**, 1095 (1980).
[13] A. Barthelemy, S. Maneuf, and C. Froehly, Propagation soliton et auto-confinement de faisceaux laser par non linearité optique de Kerr, Opt. Commun. **55**, 201 (1985).
[14] P. Emplit, J. Hamaide, F. Reynaud, C. Froehly, and A. Barthelemy, Picosecond steps and dark pulses through nonlinear single mode fibers, Opt. Commun. **62**, 374 (1987).
[15] D. Krökel, N. J. Halas, G. Giuliani, and D. Grischkowsky, Dark-pulse propagation in optical fibers, Phys. Rev. Lett. **60**, 29 (1988).
[16] A. M. Weiner, J. P. Heritage, R. J. Hawkins, R. N. Thurston, E. M. Kirschner, D. E. Leaird, and W. J. Tomlinson, Experimental observation of the fundamental dark soliton in optical fibers, Phys. Rev. Lett. **61**, 2445 (1988).
[17] C. Conti, A. Fratalocchi, M. Peccianti, G. Ruocco, and S. Trillo, Observation of a gradient catastrophe generating solitons, Phys. Rev. Lett. **102**, 083902 (2009).
[18] S. Barland, J. R. Tredicce, M. Brambilla, L. A. Lugiato, S. Balle, M. Giudici, T. Maggipinto, L. Spinelli, G. Tissoni, T. Knödl, M. Miller, and R. Jäger, Cavity solitons as pixels in semiconductor microcavities, Nature (London) **419**, 699–702 (2002).
[19] F. Pedaci, P. Genevet, S. Barland, M. Giudici, and J. R. Tredicce, Positioning cavity solitons with a phase mask, Appl. Phys. Lett. **89**, 221111 (2006).
[20] A. Amo, S. Pigeon, D. Sanvitto, V. G. Sala, R. Hivet, I. Carusotto, F. Pisanello, G. Leménager, R. Houdré, E. Giacobino, C. Ciuti, and A. Bramati, Polariton superfluids reveal quantum hydrodynamic solitons, Science **332**, 1167 (2011).
[21] G. Grosso, G. Nardin, F. Morier-Genoud, Y. Léger, and B. Deveaud-Plédran, Soliton instabilities and vortex street formation in a polariton quantum fluid, Phys. Rev. Lett. **107**, 245301 (2011).
[22] J. E. Rothenberg and D. Grischkowsky, Observation of the formation of an optical intensity shock and wave breaking in the nonlinear propagation of pulses in optical fibers, Phys. Rev. Lett. **62**, 531 (1989).
[23] W. Wan, S. Jia, and J. W. Fleischer, Dispersive superfluid-like shock waves in nonlinear optics, Nat. Phys. **3**, 46–51 (2007).
[24] G. Xu, A. Mussot, A. Kudlinski, S. Trillo, F. Copie, and M. Conforti, Shock wave generation triggered by a weak background in optical fibers, Opt. Lett. **41**, 2656 (2016).
[25] T. Bienaimé, M. Isoard, Q. Fontaine, A. Bramati, A. M. Kamchatnov, Q. Glorieux, and N. Pavloff, Quantitative analysis of shock wave dynamics in a fluid of light, Phys. Rev. Lett. **126**, 183901 (2021).
[26] P. Azam, A. Fusaro, Q. Fontaine, J. Garnier, A. Bramati, A. Picozzi, R. Kaiser, Q. Glorieux, and T. Bienaimé, Dissipation-enhanced collapse singularity of a nonlocal fluid of light in a hot atomic vapor, Phys. Rev. A **104**, 013515 (2021).
[27] F. T. Arecchi, G. Giacomelli, P. L. Ramazza, and S. Residori, Vortices and defect statistics in two-dimensional optical chaos, Phys. Rev. Lett. **67**, 3749 (1991).
[28] G. A. Swartzlander and C. T. Law, Optical vortex solitons observed in Kerr nonlinear media, Phys. Rev. Lett. **69**, 2503 (1992).
[29] M. Vaupel, K. Staliunas, and C. O. Weiss, Hydrodynamic phenomena in laser physics: Modes with flow and vortices behind an obstacle in an optical channel, Phys. Rev. A **54**, 880 (1996).
[30] K. G. Lagoudakis, M. Wouters, M. Richard, A. Baas,

I. Carusotto, R. André, L. S. Dang, and B. Deveaud-Plédran, Quantized vortices in an exciton–polariton condensate, Nat. Phys. **4**, 706–710 (2008).
[31] G. Roumpos, M. D. Fraser, A. Löffler, S. Höfling, A. Forchel, and Y. Yamamoto, Single vortex–antivortex pair in an exciton-polariton condensate, Nat. Phys. **7**, 129–133 (2011).
[32] G. Nardin, K. G. Lagoudakis, B. Pietka, F. Morier-Genoud, Y. Léger, and B. Deveaud-Plédran, Selective photoexcitation of confined exciton-polariton vortices, Phys. Rev. B **82**, 073303 (2010).
[33] G. Nardin, G. Grosso, Y. Léger, B. Pietka, F. Morier-Genoud, and B. Deveaud-Plédran, Hydrodynamic nucleation of quantized vortex pairs in a polariton quantum fluid, Nat. Phys. **7**, 635–641 (2011).
[34] D. Sanvitto, S. Pigeon, A. Amo, D. Ballarini, M. De Giorgi, I. Carusotto, R. Hivet, F. Pisanello, V. G. Sala, P. S. S. Guimaraes, R. Houdré, E. Giacobino, C. Ciuti, A. Bramati, and G. Gigli, All-optical control of the quantum flow of a polariton condensate, Nat. Photon. **5**, 610–614 (2011).
[35] C. Antón, G. Tosi, M. D. Martín, L. Viña, A. Lemaître, and J. Bloch, Role of supercurrents on vortices formation in polariton condensates, Opt. Express **20**, 16366 (2012).
[36] L. Dominici, G. Dagvadorj, J. M. Fellows, D. Ballarini, M. D. Giorgi, F. M. Marchetti, B. Piccirillo, L. Marrucci, A. Bramati, G. Gigli, M. H. Szymańska, and D. Sanvitto, Vortex and half-vortex dynamics in a nonlinear spinor quantum fluid, Sci. Adv. **1**, e1500807 (2015).
[37] A. Amo, J. Lefrère, S. Pigeon, C. Adrados, C. Ciuti, I. Carusotto, R. Houdré, E. Giacobino, and A. Bramati, Superfluidity of polaritons in semiconductor microcavities, Nat. Phys. **5**, 805 (2009).
[38] C. Michel, O. Boughdad, M. Albert, P.-E. Larré, and M. Bellec, Superfluid motion and drag-force cancellation in a fluid of light, Nat. Commun. **9**, 2108 (2018).
[39] T. W. Neely, A. S. Bradley, E. C. Samson, S. J. Rooney, E. M. Wright, K. J. H. Law, R. Carretero-González, P. G. Kevrekidis, M. J. Davis, and B. P. Anderson, Characteristics of two-dimensional quantum turbulence in a compressible superfluid, Phys. Rev. Lett. **111**, 235301 (2013).
[40] G. Gauthier, M. T. Reeves, X. Yu, A. S. Bradley, M. A. Baker, T. A. Bell, H. Rubinsztein-Dunlop, M. J. Davis, and T. W. Neely, Giant vortex clusters in a two-dimensional quantum fluid, Science **364**, 1264 (2019).
[41] S. P. Johnstone, A. J. Groszek, P. T. Starkey, C. J. Billington, T. P. Simula, and K. Helmerson, Evolution of large-scale flow from turbulence in a two-dimensional superfluid, Science **364**, 1267 (2019).
[42] M. T. Reeves, K. Goddard-Lee, G. Gauthier, O. R. Stockdale, H. Salman, T. Edmonds, X. Yu, A. S. Bradley, M. Baker, H. Rubinsztein-Dunlop, M. J. Davis, and T. W. Neely, Turbulent relaxation to equilibrium in a two-dimensional quantum vortex gas, Phys. Rev. X **12**, 011031 (2022).
[43] A. S. Bradley and B. P. Anderson, Energy spectra of vortex distributions in two-dimensional quantum turbulence, Phys. Rev. X **2**, 041001 (2012).
[44] M. Gałka, P. Christodoulou, M. Gazo, A. Karailiev, N. Dogra, J. Schmitt, and Z. Hadzibabic, Emergence of isotropy and dynamic scaling in 2d wave turbulence in a homogeneous Bose gas, Phys. Rev. Lett. **129**, 190402 (2022).
[45] P. M. Chesler, H. Liu, and A. Adams, Holographic vortex liquids and superfluid turbulence, Science **341**, 368 (2013).
[46] S. Nazarenko, M. Onorato, and D. Proment, Bose-Einstein condensation and Berezinskii-Kosterlitz-Thouless transition in the two-dimensional nonlinear Schrödinger model, Phys. Rev. A **90**, 013624 (2014).
[47] N. Navon, A. L. Gaunt, R. P. Smith, and Z. Hadzibabic, Emergence of a turbulent cascade in a quantum gas, Nature (London) **539**, 72–75 (2016).
[48] A. V. Mamaev, M. Saffman, and A. A. Zozulya, Propagation of dark stripe beams in nonlinear media: Snake instability and creation of optical vortices, Phys. Rev. Lett. **76**, 2262 (1996).
[49] D. Vocke, K. Wilson, F. Marino, I. Carusotto, E. M. Wright, T. Roger, B. P. Anderson, P. Öhberg, and D. Faccio, Role of geometry in the superfluid flow of nonlocal photon fluids, Phys. Rev. A **94**, 013849 (2016).
[50] A. Maître, F. Claude, G. Lerario, S. Koniakhin, S. Pigeon, D. Solnyshkov, G. Malpuech, Q. Glorieux, E. Giacobino, and A. Bramati, Spontaneous generation, enhanced propagation and optical imprinting of quantized vortices and dark solitons in a polariton superfluid: Towards the control of quantum turbulence, EPL **134**, 24004 (2021).
[51] A. Eloy, O. Boughdad, M. Albert, P.-É. Larré, F. Mortessagne, M. Bellec, and C. Michel, Experimental observation of turbulent coherent structures in a superfluid of light, EPL **134**, 26001 (2021).
[52] K. A. Sitnik, S. Alyatkin, J. D. Töpfer, I. Gnusov, T. Cookson, H. Sigurdsson, and P. G. Lagoudakis, Spontaneous formation of time-periodic vortex cluster in nonlinear fluids of light, Phys. Rev. Lett. **128**, 237402 (2022).
[53] R. Panico, P. Comaron, M. Matuszewski, A. S. Lanotte, D. Trypogeorgos, G. Gigli, M. De Giorgi, V. Ardizzone, D. Sanvitto, and D. Ballarini, Onset of vortex clustering and inverse energy cascade in dissipative quantum fluids, Nat. Photon. **17**, 451 (2023).
[54] M. Abobaker, W. Liu, T. Aladjidi, A. Bramati, and Q. Glorieux, Inverse energy cascade in two-dimensional quantum turbulence in a fluid of light (2022).
[55] N. Šantić, A. Fusaro, S. Salem, J. Garnier, A. Picozzi, and R. Kaiser, Nonequilibrium precondensation of classical waves in two dimensions propagating through atomic vapors, Phys. Rev. Lett. **120**, 055301 (2018).
[56] P. Azam, A. Griffin, S. Nazarenko, and R. Kaiser, Vortex creation, annihilation, and nonlinear dynamics in atomic vapors, Phys. Rev. A **105**, 043510 (2022).
[57] J. F. Nye and M. V. Berry, Dislocations in wave trains, Proc. R. Soc. Lond. A **336**, 165 (1974).
[58] J. F. Nye, The motion and structure of dislocations in wavefronts, Proc. R. Soc. Lond. A **378**, 219 (1981).
[59] I. Freund, Saddles, singularities, and extrema in random phase fields, Phys. Rev. E **52**, 2348 (1995).
[60] G. P. Karman, M. W. Beijersbergen, A. van Duijl, and J. P. Woerdman, Creation and annihilation of phase singularities in a focal field, Opt. Lett. **22**, 1503 (1997).
[61] M. Berry, Much ado about nothing: optical dislocation lines (phase singularities, zeros, vortices...), in *A Half-Century of Physical Asymptotics and Other Diversions* (World Scientific, 2017) Chap. 1.3, pp. 42–46.
[62] N. N. Rozanov, S. V. Fedorov, and A. N. Shatsev, Energy-flow patterns and bifurcations of two-dimensional cavity solitons, J. Exp. Theor. Phys. **98**, 427 (2004).

[63] J. F. Nye, J. V. Hajnal, and J. H. Hannay, Phase saddles and dislocations in two-dimensional waves such as the tides, Proc. R. Soc. Lond. A **417**, 7 (1988).

[64] The fact that I_{V} is an integer is known as the Onsager-Feynman quantization condition, see [75, 76].

[65] Vortices are also named wavefront dislocations [57] or amphidromic points (a terminology used in oceanography).

[66] In many physical situations vortices with $|I_{\mathrm{V}}|$ larger than unity are unstable.

[67] Higher values of I_{P} can be reached [77, 78], but the associated flows are non-generic and typically structurally unstable.

[68] It is worth stressing that, what is commonly referred to as the vorticity in the context of the two dimensional xy model, is actually the Poincaré-Hopf index, see e.g., Refs. [79, 80].

[69] Y. S. Kivshar and G. P. Agrawal, *Optical Solitons, From Fibers to Photonic Crystals* (Academic, New York, 2003).

[70] See Supplemental Material which presents the experimental apparatus and the parameters relevant for a realisation of the configuration discussed in the text, discusses the numerical simulation and the experimental observation of the Bristol mechanism, study the possibility to cast the fold-Hopf bifurcation under a potential form, and quotes the additional references [81–87].

[71] S. H. Strogatz, *Nonlinear Dynamics and Chaos: With Applications to Physics, Biology, Chemistry, and Engineering*, second edition ed. (Westview Press, a member of the Perseus Books Group, Boulder, CO, 2015).

[72] J. Guckenheimer and P. Holmes, *Nonlinear oscillations, dynamical systems, and bifurcations of vector fields*, 7th ed., Applied mathematical sciences, Vol. 42 (Springer, New York, 2002).

[73] Y. A. Kuznetsov, *Elements of Applied Bifurcation Theory*, 3rd ed., Applied Mathematical Sciences, Vol. 112 (Springer, New York, 2004).

[74] N. Shvartsman and I. Freund, Speckle spots ride phase saddles sidesaddle, Opt. Comm. **117**, 228 (1995).

[75] L. Onsager, Statistical hydrodynamics, Nuovo Cim. **6**, 279 (1949).

[76] R. P. Feynman, Application of quantum mechanics to liquid helium, in *Progress in Low Temperature Physics*, Vol. 1, edited by C. J. Gorter (Elsevier, 1955) Chap. II, pp. 17–53.

[77] G. Scheuermann, H. Hagen, H. Kruger, M. Menzel, and A. Rockwood, Visualization of higher order singularities in vector fields, in *Proceedings. Visualization '97 (Cat. No. 97CB36155)* (1997) pp. 67–74.

[78] I. Freund and A. Belenkiy, Higher-order extrema in two-dimensional wave fields, J. Opt. Soc. Am. A **17**, 434 (2000).

[79] J. M. Kosterlitz and D. J. Thouless, Ordering, metastability and phase transitions in two-dimensional systems, J. Phys. C: Solid State Phys. **6**, 1181 (1973).

[80] J. M. Kosterlitz, The critical properties of the two-dimensional xy model, J. Phys. C: Solid State Phys. **7**, 1046 (1974).

[81] P. Siddons, C. S. Adams, C. Ge, and I. G. Hughes, Absolute absorption on rubidium D lines: comparison between theory and experiment, J. Phys. B: At. Mol. Opt. Phys. **41**, 155004 (2008).

[82] I. H. Agha, C. Giarmatzi, Q. Glorieux, T. Coudreau, P. Grangier, and G. Messin, Time-resolved detection of relative-intensity squeezed nanosecond pulses in an ^{87}Rb vapor, New J. Phys. **13**, 043030 (2011).

[83] Q. Baudouin, R. Pierrat, A. Eloy, E. J. Nunes-Pereira, P.-A. Cuniasse, N. Mercadier, and R. Kaiser, Signatures of Lévy flights with annealed disorder, Phys. Rev. E **90**, 052114 (2014).

[84] D. A. Steck, Rubidium 87 D line data, available online at, `https://steck.us/alkalidata/` (2021).

[85] L. Wu, X. Yuan, D. Ma, Y. Zhang, W. Huang, Y. Ge, Y. Song, Y. Xiang, J. Li, and H. Zhang, Recent advances of spatial self-phase modulation in 2D materials and passive photonic device applications, Small **16**, 2002252 (2020).

[86] E. A. Kuznetsov and S. K. Turitsyn, Instability and collapse of solitons in media with a defocusing nonlinearity, Sov. Phys. JETP **67**, 1583 (1988).

[87] V. Tikhonenko, J. Christou, B. Luther-Davies, and Y. S. Kivshar, Observation of vortex solitons created by the instability of dark soliton stripes, Opt. Lett. **21**, 1129 (1996).